Interaction between x-ray and magnetic vortices

Michel van Veenendaal

Phys. Rev. B **92**, 245116 — Published 10 December 2015

DOI: 10.1103/PhysRevB.92.245116

The interaction between X-ray and magnetic vortices

Michel van Veenendaal[1,2]

[1]*Department of Physics, Northern Illinois University, DeKalb, Illinois 60115, USA*
[2]*Advanced Photon Source, Argonne National Laboratory, 9700 South Cass Avenue, Argonne, Illinois 60439, USA*

(Dated: November 10, 2015)

The interaction between two topological objects, an X-ray beam carrying orbital angular momentum (OAM) and a magnetic vortex, is studied theoretically. The resonant X-ray scattering intensity is calculated as a function of the relative position of the magnetic and X-ray vortices. For a homogeneous system, the charge scattering is zero. For magnetic scattering, the intensity profile strongly depends on the relative topological indices of the X-ray and magnetic singularities. A strong enhancement in the intensity profile is observed for equal winding factors. Additionally, the profile displays edge effects, which depend on the scattering conditions, the radial dependence of the magnetic vortex, and the Laguerre-Gaussian mode of the OAM X-ray beam. The potential of resonant OAM X-ray scattering from magnetic vortices opens the door to study the dynamics and switching of magnetic vortices.

I. INTRODUCTION

Photons in singular electromagnetic beams with a cork-screw-like phase distribution carry an orbital angular momentum (OAM) of $l\hbar$[1]. In the visible part of the electromagnetic spectrum, this intriguing property has led to a number of new applications, such as optical manipulation[2,3], multiplexing of information for terabit free-space data transmission[4], and to generate an atomic vortex state in a Bose-Einstein condensate[5]. In the X-ray region, tremendous progress has been made generating vortices. Initially, vortices were created using conventional methods of manipulating X-ray beams such as apertures and zone plates[6,7]. More recently, the attention has shifted towards the direct generation of X-ray vortices. OAM X-ray beams are produced as higher harmonics in a helical undulator[8,9], through the interaction of an electron beam with a seed laser in a helical undulator[10–12], or via echo-enabled harmonic generation[13]. This has led to significantly more intense OAM X-ray beams. Although the generation of OAM beams is of great interest by itself, the potential for applications using short-wavelength OAM beams has been limited. Interest has focused on absorption[14] and photoionization[15]. In X-ray absorption, taking the difference between positive and negative OAM states can lead to substantial dichroic effects[14]. Experimentally, the use of orbital-angular momentum to induce dichroic effects has been demonstrated for electron beams[16].

In this Letter, we look at the interaction between an OAM X-ray beam and another singular object, namely, a magnetic vortex[17,18]. In a magnetic vortex, the magnetization curls around the center, see Fig. 1(a). As OAM beams, they can be characterized in terms of a topological index or winding number. These topological magnetic states are not only of scientific interest, but also have potential applications in spintronics if their topological charges can be fully manipulated. These magnetic vortices have been studied by, for example, magnetic-force microscopy[18], Kerr spectroscopy[19], and photoemission electron microscopy[20]. Here, we discuss the unique features resulting from the interaction between two singular objects by simulating the intensity of an OAM X-ray beam that resonantly scatters of a magnetic vortex. A strong dependence on their relative topological indices is found and the appearance of a singularity in the scattering intensity as a function of position is observed for matching winding numbers.

II. THEORY

The vector potential for a linearly-polarized Laguerre-Gaussian beam carrying orbital angular momentum propagating in the direction of the wavevector $\mathbf{k}$[1] can be written as

$$\mathbf{A}_{nl}(\mathbf{r}) = \boldsymbol{\epsilon} A_{nl}(\rho_{\mathbf{r}}) e^{i\mathbf{k}\cdot\mathbf{r}+il\varphi_{\mathbf{r}}}, \tag{1}$$

where $\boldsymbol{\epsilon}$ is the polarization vector. The integer l is the winding number or topological index describing the orbital angular momentum carried by the beam. The OAM beam is defined in terms of coordinates with respect to its center. The vector $\boldsymbol{\rho}_{\mathbf{r}} = \mathbf{r} - (\mathbf{r}\cdot\boldsymbol{e}_{\mathbf{k}})\boldsymbol{e}_{\mathbf{k}}$ is perpendicular to the unit vector in the propagation direction $\boldsymbol{e}_{\mathbf{k}} = \mathbf{k}/k$. The amplitude of the beam is a function of the distance to the center of the beam $\rho_{\mathbf{r}} = |\boldsymbol{\rho}_{\mathbf{r}}|$. In the long Rayleigh range, the transverse amplitude is given by[1,21]

$$A_{nl}(\rho) = a_{nl}\sqrt{\frac{2n!}{\pi r_0^2 (n+l)!}}\left(\frac{\sqrt{2}\rho}{r_0}\right)^{|l|} e^{-\frac{\rho^2}{r_0^2}} L_n^l\left(\frac{2\rho^2}{r_0^2}\right). \tag{2}$$

The beam is normalized such that the strength only depends on the factor a_{nl},

$$\int_0^{2\pi} d\varphi \int_0^{\infty} d\rho\, \rho |A_{nl}(\rho)|^2 = a_{nl}^2. \tag{3}$$

The width of the beam is determined by r_0 and $L_n^l(x)$ is an associated Laguerre polynomial of order n. The order

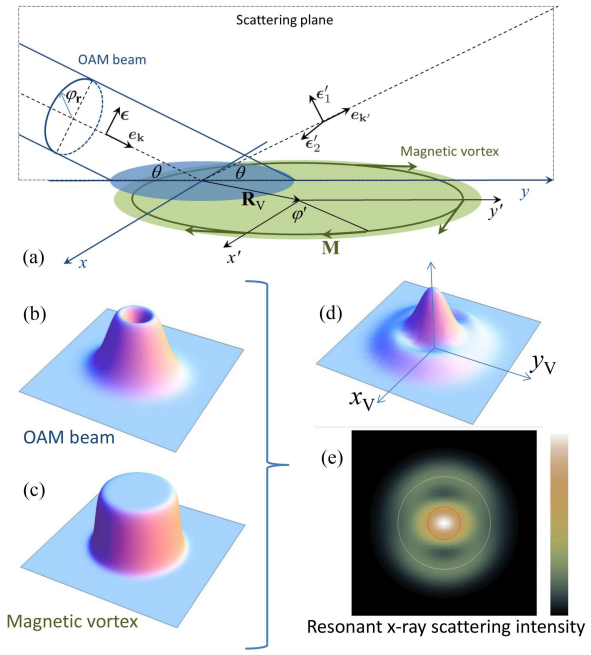

FIG. 1: (a) Schematic diagram of the resonant X-ray scattering of a Laguerre-Gaussian beam carrying orbital momentum (blue) on a magnetic vortex (green). The situation is shown for π scattering where the incoming polarization $\boldsymbol{\epsilon}$ is in the scattering plane and the outgoing polarization is not measured. (b) The intensity of the beam $|\mathbf{A}_{0,\pm1}(\mathbf{r})|$ at the sample surface. (c) The magnitude $|\mathbf{M}|$ of the magnetic vortex in the sample. (d) The intensity I^1_{01} of the resonant magnetic X-ray scattering as a function of the relative displacement on the sample surface $\mathbf{R}_V$ of the center of the magnetic vortex relative to the center of the Laguerre-Gaussian beam. The calculations are done for π polarized light and an angle of incidence of 60°. (e) Density plot of I^1_{01}. The colors for the relative intensities are given in the bar on the right side.

n specifies the number of nodes in the beam in addition to a (possible) node at the center of the beam. The vector $\boldsymbol{\rho}_\mathbf{r}$ can be expressed in terms of the linear polarization vectors of the vector potential $\boldsymbol{\rho}_\mathbf{r} = \cos\varphi_\mathbf{r}\boldsymbol{e}_\pi + \cos\varphi_\mathbf{r}\boldsymbol{e}_\sigma$, where $\boldsymbol{e}_\pi$ and $\boldsymbol{e}_\sigma$ are perpendicular to $\mathbf{k}$ and in and perpendicular to the scattering plane, respectively, see Fig. 1(a). The orbital angular momentum appears in the dependence of the X-ray beam on the phase $\varphi_\mathbf{r}$. For the case of $nl = 0, \pm1$, the vector potential reduces to

$$\mathbf{A}_{0,\pm1}(\mathbf{r}) = \boldsymbol{\epsilon}\frac{2}{\sqrt{\pi}}\rho_\mathbf{r} e^{-\frac{\rho^2_\mathbf{r}}{r^2_0}+i\mathbf{k}\cdot\mathbf{r}\pm i\varphi_\mathbf{r}}, \tag{4}$$

giving a typical donut-like intensity distribution of the magnitude of the vector potential, see Fig. 1(b).

The resonant scattering amplitude is given by[22]

$$I_{nl}(\omega) = \sum_{\alpha=1,2}\left|\sum_\mathbf{R}\mathcal{F}_\mathbf{R}(\omega,\alpha)E_{nl}(\rho_\mathbf{R})e^{i(\mathbf{k}-\mathbf{k}')\cdot\mathbf{R}+il\varphi_\mathbf{R}}\right|^2,$$

where $E_{nl} = i\omega A_{nl}$ is the electric field. We make here the assumption that the beam is much larger than the size of the atomic orbitals, which allows us to neglect variations of the vector potential across the atom. The summation variable α is over the two outgoing polarization vectors $\boldsymbol{\epsilon}'_\alpha$. When the scattering satisfies the Bragg condition, the transferred momentum equals a reciprocal lattice vector, *i.e.* $\mathbf{K} = \mathbf{k} - \mathbf{k}'$ giving $e^{i\mathbf{K}\cdot\mathbf{R}} = 1$ at the scattering centers. The local scattering amplitude in the dipole approximation is given by the Kramers-Heisenberg expression

$$\mathcal{F}_\mathbf{R}(\omega,\alpha) = \sum_m\sum_{ij}\frac{\langle g|\boldsymbol{\epsilon}'_\alpha\cdot\mathbf{r}_j|m\rangle\langle m|\boldsymbol{\epsilon}\cdot\mathbf{r}_i|g\rangle}{\hbar\omega + E_g - E_m + i\Gamma_m/2}, \tag{5}$$

where $|g\rangle$ is the ground state and Γ_m is the intermediate state lifetime broadening. The summation m goes over the resonant x-ray scattering intermediate states and the summations i and j are over the electrons at the site where the scattering occurs.

By using a recoupling, we can separate the scattering amplitude into a geometric term determined by the scattering geometry and a fundamental scattering amplitude related to the local electronic and magnetic properties[22]

$$\mathcal{F}_\mathbf{R}(\omega,\alpha) = \sum_{L=0}^{2}\mathbf{T}^L(\boldsymbol{\epsilon},\boldsymbol{\epsilon}'_\alpha)\cdot\mathbf{C}^L(\hat{\mathbf{M}})F^L(\omega). \tag{6}$$

The different ranks correspond to different types of scattering: $L = 0$ is the resonant charge scattering, with $\mathbf{T}^0(\boldsymbol{\epsilon},\boldsymbol{\epsilon}'_\alpha) = \frac{1}{3}\boldsymbol{\epsilon}'^*_\alpha\cdot\boldsymbol{\epsilon}$, and $L = 1$ is magnetic scattering, with $\mathbf{T}^1(\boldsymbol{\epsilon},\boldsymbol{\epsilon}'_\alpha) = -\frac{i}{2}\boldsymbol{\epsilon}'^*_\alpha\times\boldsymbol{\epsilon}$. The $L = 2$ scattering is related to the local quadrupolar moments and usually a result of the presence of orbital ordering. We assume this latter term to be small and neglect it in the remainder. Of importance is the relative orientation of the angular dependence $\mathbf{T}^L(\boldsymbol{\epsilon},\boldsymbol{\epsilon}'_\alpha)$ relative to the direction of the local order, where $\mathbf{C}^L(\hat{\mathbf{M}})$ is a renormalized spherical harmonic in the direction $\hat{\mathbf{M}}$ of the local magnetization. In particular, we have $\mathbf{C}^0(\hat{\mathbf{M}}) = 1$ and $\mathbf{C}^1(\hat{\mathbf{M}}) = \hat{\mathbf{M}}$. The strength of the scattering is expressed in terms of fundamental scattering amplitudes $F^L(\omega)$. Defining

$$F_{q'q}(\omega) = \sum_m\frac{\langle g|D^\dagger_{q'}|m\rangle\langle m|D_q|g\rangle}{\hbar\omega + E_g - E_m + i\Gamma_m/2}, \tag{7}$$

where D_q is q'th component of the dipole operator. If the z axis of the coordinate system is parallel to the local magnetization direction $\hat{\mathbf{M}}$ then, in most symmetries, only the diagonal components $q' = q$ remain. The fundamental scattering amplitudes are then $F^0 = \sum_q F_{qq}$ and $F^1 = F_{11} - F_{-1,-1}$.

Let us first consider the charge scattering. We take a typical diffraction geometry where the angle θ of the incoming and outgoing beam with respect to the sample surface are equal, see Fig. 1(a). The incoming polarization $\boldsymbol{\epsilon} = \boldsymbol{e}_\pi$ lies in the scattering plane. The outgoing polarization is not measured and a summation is made over both polarization vectors $\boldsymbol{\epsilon}'_1 = \boldsymbol{e}'_\pi$ and $\boldsymbol{\epsilon}'_2 = \boldsymbol{e}_\sigma$. The

angular dependence is then $\mathbf{T}^0(\boldsymbol{\epsilon}, \boldsymbol{\epsilon}'_\alpha) = \frac{1}{3}\cos 2\theta\, \delta_{\alpha,1}$. If the beam size is significantly larger than the atomic distances, the summation over $\mathbf{R}$ can be replaced by an integration, giving

$$I^0_{nl}(\omega) = \left|\cos 2\theta F^0(\omega) \int d\mathbf{R}\, E_{nl}(\rho_\mathbf{R}) e^{il\varphi_\mathbf{R}}\right|^2. \quad (8)$$

However, if the system is homogeneous, the integral is zero due to the presence of the complex phase factor of the angular momentum in the x-ray beam. There is therefore no coherent charge scattering from an X-ray beam carrying orbital angular momentum for a homogeneous system.

Let us now focus our attention to magnetic scattering. Since the polarization is linear, let us switch to cartesian coordinates. The nonzero scattering amplitude is then $F^1 = F_{xy} - F_{yx}$, which is calculated with the magnetization direction at a particular point inside the vortex as the z axis. The change in scattering strength due to the relative orientation of the magnetization is determined by the angular dependence $\mathbf{T}^1(\boldsymbol{\epsilon}, \boldsymbol{\epsilon}'_\alpha) \cdot \hat{\mathbf{M}}$. In cartesian coordinates and for π-polarized incoming radiation, the polarization dependence is given by $\mathbf{T}^1(\boldsymbol{\epsilon}, \boldsymbol{\epsilon}'_1) = \frac{1}{2}\boldsymbol{e}'_\pi \times \boldsymbol{e}_\pi = -\frac{1}{2}\boldsymbol{e}_x \sin 2\theta$ and $\mathbf{T}^1(\boldsymbol{\epsilon}, \boldsymbol{\epsilon}'_2) = \frac{1}{2}\boldsymbol{e}'_\sigma \times \boldsymbol{e}_\pi = -\frac{1}{2}\boldsymbol{e}_\mathbf{k}$.

III. RESULTS

In order to better understand the interaction of the OAM X-ray beam with a topological magnetic state, let us study the example of a planar magnetic vortex with cylindrical symmetry rotating clockwise with respect to the surface normal, see Fig. 1(a). The magnetization is then given by

$$\mathbf{M} = M(\rho')\hat{\mathbf{M}}(\varphi'), \text{ with } \hat{\mathbf{M}}(\varphi') = \sin\varphi' \boldsymbol{e}_x - \cos\varphi' \boldsymbol{e}_y, (9)$$

where the cylindrical coordinates of the magnetic vortex $\mathbf{r}' = \mathbf{r} - \mathbf{R}_V$, where $\mathbf{R}_V$ is the center of the vortex, are shifted with respect to the origin which is determined by the position where the center of the X-ray beam hits the sample, see Fig. 1(a). For the radial function, we take $M(\rho') = \frac{1}{2}[1 - \tanh\alpha(\rho' - r_v)]$, where r_v is the radius of the magnetic vortex. This is essentially a smoothened step function. Unless noted otherwise, $\alpha = 5$. The magnitude of the magnetization is shown in Fig. 1(c). The angular dependence is then given by

$$f_1(\theta, \varphi') = \mathbf{T}^1(\boldsymbol{\epsilon}, \boldsymbol{\epsilon}'_1) \cdot \hat{\mathbf{M}}(\varphi') = -\frac{1}{2}\sin\varphi' \sin 2\theta \quad (10)$$

$$f_2(\theta, \varphi') = \mathbf{T}^1(\boldsymbol{\epsilon}, \boldsymbol{\epsilon}'_2) \cdot \hat{\mathbf{M}}(\varphi') = \frac{1}{2}\cos\varphi' \cos\theta. \quad (11)$$

If the incoming light has a polarization $\boldsymbol{\epsilon} = \boldsymbol{e}_\sigma$, then f_1 changes sign and $f_2 = 0$. The magnetic scattering intensity is given by

$$I^1_{nl}(\omega) = \sum_{\alpha=1,2} \left|F^1(\omega) \int d\mathbf{R}\, f_\alpha(\theta, \varphi') M(\rho') E_{nl}(\rho_\mathbf{R}) e^{il\varphi_\mathbf{R}}\right|^2.$$

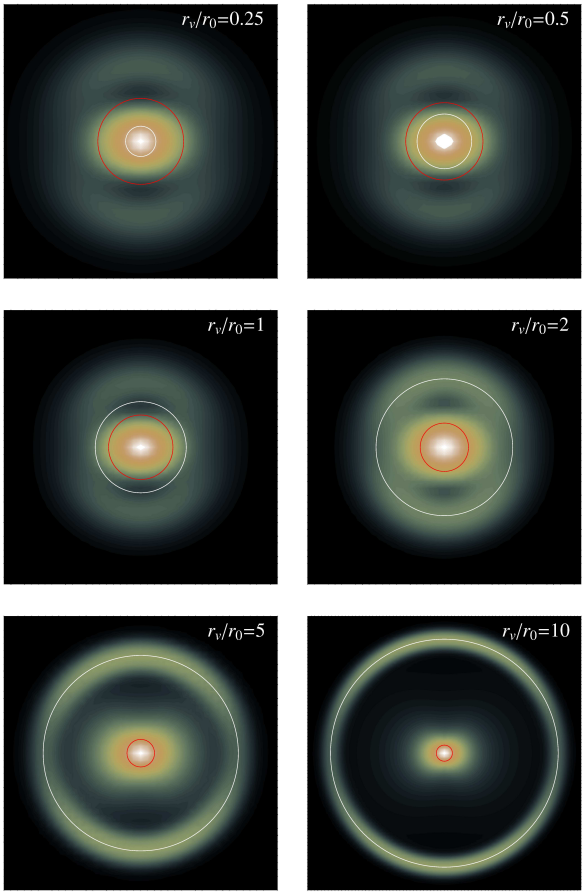

FIG. 2: The intensity of I^1_{01} of the resonant magnetic X-ray scattering as a function of the relative displacement on the sample surface $\mathbf{R}_V$ of the center of the magnetic vortex relative to the center of the Laguerre-Gaussian beam for different relative sizes r_v/r_0, where r_v (indicated as a white circle) is the size of the magnetic vortex and r_0 the width of the X-ray beam (indicated by a red circle with a radius $r_0/\sqrt{2}$, where the intensity is maximum) . The calculations are done for π polarized light and an angle of incidence of 60°.

A typical calculation of the magnetic scattering is given in Figs. 1(d) and (e), where the intensity is plotted as a function of the relative displacement $\mathbf{R}_V$ of the centers of the X-ray and magnetic vortices. The Laguerre-Gaussian mode is $nl = 01$, which has the same topological index as the magnetic vortex. The angle of incidence θ is 60° and the incoming polarization vector is $\boldsymbol{e}_\pi$. The relative sizes of the vortices are determined by the ratio r_v/r_0, where the maximum of the Laguerre-Gaussian beam at $r_0/\sqrt{2}$ is indicated by the red circle in the Figure. The most noticeable feature is the strong singularity for $\mathbf{R}_V = 0$, when there is a constructive interference in the resonance scattering. Additional intensity can also be observed due to edge effects when the two vortices do not entirely overlap and resonant scattering intensity from one side of the OAM beam is not cancelled by that on the opposite site.

Figure 2 shows the dependence of the resonant X-ray

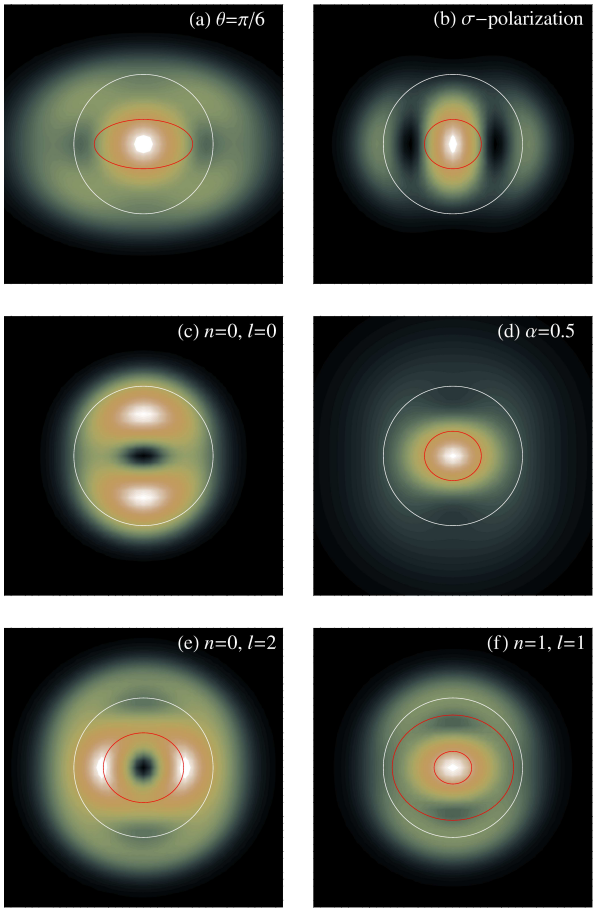

FIG. 3: The changes in intensity of I^1_{nl} of the resonant magnetic scattering as a function of the relative displacement on the sample surface $\mathbf{R}_V$ of the magnetic vortex relative to the Laguerre-Gaussian beam when changing the experiment from a π-polarized $nl = 01$ Laguerre-Gaussian beam at a 60° angle of incidence with $r_v/r_0 = 2$: (a) 30° angle of incidence, (b) σ-polarization, (c) $nl = 00$, (d) a more slowly varying magnetic vortex ($\alpha = 0.5$, see text) (e) $nl = 02$, (f) $nl = 11$ (note that there are now two maxima in the Laguerre-Gaussian beam).

scattering intensity as a function of their relative displacement for different relative sizes r_v/r_0 of the vortices for identical scattering conditions. All intensity profiles have the singularity in the intensity for $\mathbf{R}_V = 0$. Additional intensity is observed resulting from the variations in the overlap in the radial dependence of the X-ray and magnetic vortices. An interesting situation occurs for large r_v/r_0, where the intensity strongly drops when the OAM beam is inside the magnetic vortex but not close to the center or the edge. In this region, the magnetization in the beam can be considered almost constant since the size of the X-ray beam is small relative to the size of the magnetic vortex. However, due to the presence of a phase in the X-ray beam, the resonant scattering amplitude is very small.

The scattering profile can be changed by varying the scattering conditions or the Laguerre-Gaussian modes, see Fig. 3. Figure 3(a) shows the effect of changing the angle of incidence from 60° to 30°, for the same scattering conditions as in Fig. 2 and $r_v/r_0 = 2$. Due to the more grazing angle of incidence, the intensity profile simply becomes more elongated. For σ-polarized light and $\theta = 60°$, see Fig. 3(b), $f_2(\theta, \varphi')$ is zero and the scattering profile becomes strongly asymmetric with the largest intensity in the direction of the scattering plane.

Let us now look at different Laguerre-Gaussian modes. For $n = 0$ and $l = 0$, the beam has a simple Gaussian radial dependence with no phase dependence. When the centers of the vortices are at the same position ($\mathbf{R}_V = 0$), the intensity goes to zero and no center singularity is observed, see Fig. 3(c). The phase of the magnetic vortex cancels the scattering amplitudes coming from opposite sides of the Laguerre-Gaussian beam. However, when the vortices are displaced with respect to each other, a finite magnetic scattering intensity is observed since the cancellation is not complete. However, since these are edge effects, the strenghth of this scattering is relatively weak. Additionaly the scattering intensity due to edge effects depends on the sharpness of the edge of the magnetic vortex. If the magnetization changes more smoothly then the edge effects are less prominent, see Fig. 3(d), which is calculation using $\alpha = 0.5$ in the radial dependence $M(\rho')$ of the magnetization. The mode is $nl = 01$ and 3(d) should be compared with Fig. 1(e).

Interesting effects occur when increasing the n and l values. For $n = 0$ and $l = 2$, the radial intensity of A_{02} is comparable to A_{01} with its maximum shifted to a slightly larger ρ. However, the winding number l has increased by 1, leading to the disappearance of the singularity at $\mathbf{R}_V = 0$ due to the different topological indices of the X-ray and magnetic vortices, see Fig. 3(e). Increasing n has a less drastic effect. The Laguerre-Gaussian beam with $n = 1$ and $l = 1$ has two maxima in the radial dependence, indicated in red in Fig. 3(f). Although the detailed dependence is different, the general behavior of the scattering intensity is comparable to that in Fig. 1(e) with $nl = 01$.

So far, the focus was on the possibility of detecting magnetic vortices using X-ray beams carrying orbital angular momentum (OAM). Here, we take a closer look at the effects of chirality. For a planar magnetic vortex, the direction of the magnetization is given by

$$\hat{\mathbf{M}}(\varphi) = \cos\varphi' \boldsymbol{e}_x + \sin\varphi' \boldsymbol{e}_y. \tag{12}$$

where φ is the polar angle on the sample surface. The value of φ' is given by[23,24]

$$\varphi' = n\varphi + c\frac{\pi}{2} \tag{13}$$

where $n = \pm 1$ for vortices and antivortices, respectively; c is the chirality. For a vortex ($n = 1$), the stable values for the chirality are $c = \pm 1$. In the main text, the vortex rotated clockwise and has a chirality of $c = -1$. In resonant X-ray scattering, the square of the magnetic

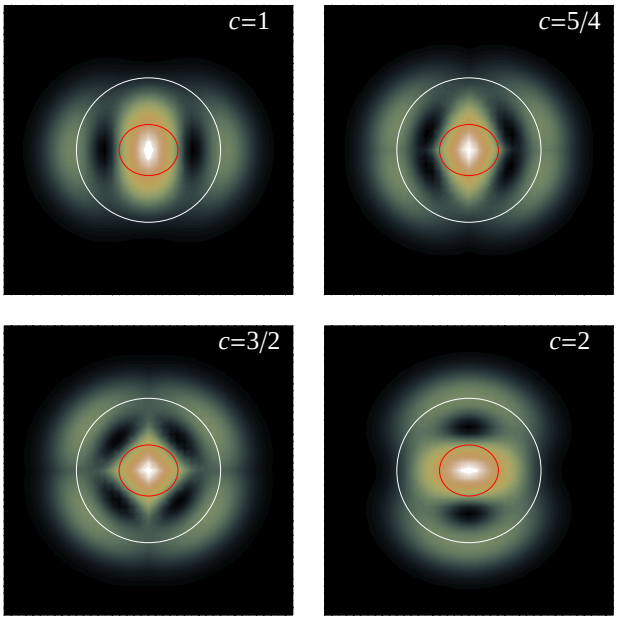

FIG. 4: The intensity of I_{01}^{1} of the resonant magnetic X-ray scattering as a function of the relative displacement on the sample surface $\mathbf{R}_V$ of the center of a magnetic antivortex ($n = -1$) relative to the center of the Laguerre-Gaussian beam for different chiralities c. The radii of the magnetic vortex (r_V) and the X-ray beam ($r_0/\sqrt{2}$) are indicated by the white and red circles, respectively. The calculations are done for σ-polarized light and an angle of incidence of 60°.

scattering amplitude is measured and the signal is independent of the sign of the chirality. The situation is more interesting for antivortices ($n = -1$), where the allowed values are $-2 < c \leq 2$. The additional possibilities occur because an antivortex is not invariant with respect to rotations around the center of the vortex and the change in chirality corresponds to a rotation around this center. Figure 4 shows the dependence of the resonant scattering on the chirality of the antivortex. The sensitivity to the chirality comes from the presence of the scattering plane defined by the incoming and outgoing polarization vectors. Note that the intensity profile is not entirely cylindrically symmetric due to the presence of the scattering plane defined by the propagation and polarization vectors. Apart from some differences due to the scattering conditions, the intensity profile follows the rotation of the magnetic vortex due to the change in chirality.

IV. CONCLUSIONS

It has been shown that the interaction between the topological phases of X-ray and magnetic vortices lead to a finite resonant X-ray scattering amplitude. For equal winding numbers, the strongest intensity occurs when the centers of the vortices coincide. Additionally, off-center intensity can occur due to an incomplete cancellation of the resonant scattering. The increased flux and flexibility of OAM X-ray beams created using undulator techniques can provide interesting opportunities in the field of topological physics. Possible application could occur in the area of vortex dynamics and switching between different topological indices. Whereas this initial study focused on the scattering amplitude of a single planar magnetic vortex, more study needs to be done on the interaction with magnetic vortex lattices and the possible interaction between OAM X-ray beams and magnetic skyrmions.

V. ACKNOWLEDGMENTS

Discussions with Ian McNulty and Shigemi Sasaki are acknowledged. This work was supported by the U. S. Department of Energy (DOE), Office of Basic Energy Sciences, Division of Materials Sciences and Engineering under Award No. DE-FG02-03ER46097, the time-dependent x-ray spectroscopy collaboration as part of the Computational Materials Science Network (CMSCN) under grants DE-FG02-08ER46540 and DE-SC0007091, and NIU Institute for Nanoscience, Engineering, and Technology. Work at Argonne National Laboratory was supported by the U. S. DOE, Office of Science, Office of Basic Energy Sciences, under contract No. DE-AC02-06CH11357.

[1] L. Allen, M. W. Beijersbergen, R. J. C. Spreeuw, and J. P. Woerdman, Phys. Rev. A **45**, 8185 (1992).
[2] H. He, M. E. J. Friese, N. R. Heckenberg, and H. Rubinsztein-Dunlop, Phys. Rev. Lett. **75**, 826 (1995).
[3] M. Padgett and R. Bowman, Nat. Photonics **5**, 343 (2011).
[4] J. Wang *et al*, Nat. Photonics **6**, 488 (2012).
[5] M. F. Andersen, C. Ryu, P. Cladé, V. Natarajan, A. Vaziri, K. Helmerson, and W. D. Phillips, Phys. Rev. Lett. **97**, 170406 (2006).
[6] A. G. Peele, P. J. McMahon, D. Paterson, C. Q. Tran, A. P. Mancuso, K. A. Nugent, J. P. Hayes, E. Harvey, B. Lai, and I. McNulty, Opt. Lett. **27**, 1752 (2002).
[7] S. Rehbein, S. Heim, P. Guttmann, S. Werner, and G. Schneider, Phys. Rev. Lett. **103**, 110801 (2009).
[8] S. Sasaki and I. McNulty, Phys. Rev. Lett. **100**, 124801 (2008).
[9] J. Bahrdt, K. Holldack, P. Kuske, R. Müller, M. Scheer, and P. Schmid, Phys. Rev. Lett. **111**, 034801 (2013).
[10] E. Hemsing, A. Marinelli, and J. B. Rosenzweig, Phys. Rev. Lett. **106**, 164803 (2011).
[11] E. Hemsing, A. Knyazik, M. Dunning, D. Xiang, A. Marinelli, C. Hast, and J. B. Rosenzweig, Nat. Phys. **9**, 549 (2013).
[12] P. R. Ribič, D. Gauthier, and G. De Ninno, Phys. Rev. Lett. **112**, 203602 (2014).
[13] E. Hemsing and A. Marinelli, Phys. Rev. Lett. **109**, 224801

(2012).
[14] M. van Veenendaal and I. McNulty, Phys. Rev. Lett. **98**, 157401 (2007).
[15] A. Picón, J. Mompart, J. R. Vázquez de Aldana, L. Plaja, G. F. Calvo, and L. Roso, Optics Express **18**, 3660 (2010).
[16] J. Verbeeck, H. Tian, and P. Schattschneider, Nature **467**, 301 (2010).
[17] S. Mühlbauer, B. Binz, F. Jonietz, C. Pfleiderer, A. Rosch, A. Neubauer, R. Georgii, and P. Böni, Science **323**, 915 (2009).
[18] T. Shinjo, T. Okuno, R. Hassdorf, K. Shigeto, and T. Ono, Science **289**, 930 (2000).
[19] R. P. Cowburn, D. K. Koltsov, A. O. Adeyeye, M. E. Welland, and D. M. Tricker, Phys. Rev. Lett. **83**, 1042 (1999).
[20] K. Y. Guslienko, X. F. Han, D. J. Keavney, R. Divan, and S. D. Bader, Phys. Rev. Lett. **96**, 067205 (2006).
[21] L. C. Dávila Romero, D. L. Andrews, and B. M., J. Opt. B **4**, S66 (2002).
[22] M. van Veenendaal, *The Theory of Inelastic Scattering and Absorption of X-rays* (Cambridge University Press, Cambridge, 2015).
[23] J. He, Z. Li, and S. Zhang, Phys. Rev. B **73**, 184408 (2006).
[24] A. Drews, B. Krüger, M. Bolte, and G. Meier, Phys. Rev. B **77**, 094413 (2008).